PREDICTION MODEL OF BLAST FURNACE MOLTEN IRON TEMPERATURE AND MOLTEN IRON SILICON CONTENT BASED ON IMPROVED ARITHMETIC OPTIMIZATION TWIN SUPPORT VECTOR MACHINE FOR REGRESSION

C.-Y. Shi [a*], P.-L. Tao [a], S.-D. Li [b], Y.-K. Wang [a], L. Zhang [a]

[a] School of Electrical and Automation Engineering, Liaoning Institute of Science and Technology, Benxi, China
[b] Special Steel Division of Benxi Steel Plate Co. Benxi, China

Abstract

The temperature and silicon content of molten blast furnace iron are directly related to its quality. Therefore, creating an effective prediction model for these parameters is crucial. To address these issues, an Improved Arithmetic Optimization Twin Support Vector Machine for Regression (LAOA-TSVR) model was developed to predict the temperature and silicon content of molten blast furnace iron. First, SPSS was used to perform a correlation analysis and identify the main influencing factors. Secondly, the model was compared with three common prediction models to verify its prediction performance: Back Propagation Neural Network (BP), Support Vector Regression (SVR), and Twin Support Vector Machine for Regression (TSVR). Preliminary results indicate that the prediction accuracy of the LAOA-TSVR model is significantly higher than that of the other models. Finally, the model was applied to the actual production process of an iron mill for a total of 200 furnaces. The results show that the hit rates for molten iron temperature and silicon content are within the error ranges of ±5% and ±0.5% at 92.12% and 92.53%, respectively, with a corresponding double-hit rate of 85.32%. The model effectively fulfills the production requirements of an iron mill and provides valuable information for the production process in the blast furnace.

Keywords: Temperature of molten iron in blast furnace; Silicon content of molten iron; Quality of molten iron, Arithmetic optimization algorithm, Twinned support vector regression

1. Introduction

Blast furnace ironmaking is a crucial aspect of iron production. The process involves a series of complex high-temperature, high-pressure physical and chemical reactions to reduce iron from iron ore and other solid iron-containing compounds. This process exhibits strong nonlinearity, multivariable dependencies, strong coupling, time variance, large time lags, and various other complex dynamic features [1]. Therefore, general traditional prediction models are difficult to further improve. Establishing an efficient and high-precision prediction model is crucial for controlling the accuracy of blast furnace production, improving ironmaking efficiency, and increasing raw material utilization.

Accurate prediction of blast furnace molten iron temperature and silicon content is critical for the steel industry's production and operation [2]. In the early stages of research, many scholars conducted extensive studies to model blast furnace molten iron quality parameters. In the late 1960s, a Japanese scholar proposed a one-dimensional mechanistic model for molten iron temperature. However, the blast furnace is a complex multi-dimensional system where the temperature and material distribution of molten iron exist not only along the vertical axis but also radially. Subsequently, other scholars have extended the one-dimensional model to address its limitations by proposing the use of multiphase flow and two-way interphase interaction, known as the "multi-fluid theory," to describe the phenomena in the lower part of the furnace, making significant progress. However, the model can only be applied under more stable furnace conditions, which presents certain limitations. In the 1980s, with the advancement of artificial intelligence technology, researchers began using related methods to study the problem. However, solving the complex blast furnace problem remained challenging. After extensive research, several models

have been proposed to predict silicon content, including a linear prediction model based on mathematical and statistical methods combined with Auto-Regressive Vector (ARX), the Vector Auto-Regressive Moving Average (VARMAX) [3,4], and an improved model combining genetic algorithm and BP neural network [5,6]. Subsequently, researchers began using the SVR algorithm to address these problems. While SVR excels in handling small samples, nonlinear regression, and high-dimensional data, its training process is slow when dealing with large-scale data [7,8]. Currently, deep learning methods are used to predict molten iron temperature and silicon content. However, deep learning models typically require a large amount of labeled data for effective training, which is expensive and inadequate for solving problems involving complex reasoning or dynamic decision-making. Furthermore, the deep learning approach requires significant computational resources, making model training and inference costly, with high hardware requirements. These factors raise the cost of applying the model. This may increase the cost of replicating the model across additional steel groups [9]. Compared to the above methods, the TSVR algorithm effectively addresses these drawbacks. It overcomes the neural networks' tendency to fall into local minima and has significant advantages in dealing with nonlinear problems, small samples, and high-dimensional data. Consequently, it has been widely researched and applied in various fields in recent years [10].

To address these issues, the research group proposes a prediction model for blast furnace molten iron end temperature and silicon content based on LAOA-TSVR, enabling efficient processing of multi-dimensional complex data [11,12]. The algorithm also solves the optimization problem under multiple constraints, ensuring a unique optimal solution, and greatly improves the model's prediction accuracy.

In the research process, the first step was to normalize the industrial trial data of an iron mill to determine the model inputs. Despite its benefits, the TSVR still cannot fully address the issue of potential numerical overflow in multidimensional data. To solve this problem, AOA was used to optimize the kernel function, tuning parameters, and penalty factors [13]. Additionally, AOA is prone to issues such as poor exploration capabilities and early convergence to non-optimal solutions [14]. Therefore, the research group introduced the Lévy algorithm to improve AOA(LAOA). The LAOA algorithm compares favorably with other well-known algorithms, such as the improved particle swarm optimization algorithm and the improved sparrow search algorithm, both based on Lévy flight algorithm, offering simpler

computation and strong global optimization capabilities [15,16]. The LAOA-TSVR not only escapes local optima and better solves multidimensional optimization problems, but also expands the parameter search range and accelerates convergence speed. To verify the predictive performance of the LAOA-TSVR model, its prediction indexes (SSR (Sum of squares of the regression)/SST(Total sum of squares), SSE(The sum of squares due to error)/SST(Total sum of squares), RMSE (Root mean squared error), MAE (Mean absolute error), and HR (Hit Rate)) were compared and analyzed against those of BP, SVR, and TSVR models. The LAOA-TSVR model was determined to have the best prediction results. Finally, the model was applied to industrial trials to assess its practical application. Given the slight variations in production processes among ironworks, the model can be tailored to accommodate these differences, ensuring high prediction accuracy. This adaptability highlights the model's robust generalizability.

2. Industrial Trials

During industrial trials, the research group used the blast furnace of an iron mill as the research object. The blast furnace production-related testing equipment and parameters of the production process were utilized to collect the required blast furnace ironmaking data for the model. These parameters mainly included: Coke ratio, Coal ratio, Wind speed, Coke load, Air permeability index, Blast furnace air volume, Blast furnace bosh gas volume, Comprehensive smelting intensity, Oxygen enrichment rate, Coke smelting intensity, Hot-air blast temperature, Comprehensive coke ratio, Furnace top pressure, Hot blast air pressure, Comprehensive load, Slag-iron ratio. The temperature of the molten iron was measured at the outlet using a temperature measuring gun (model: Heraeus LCTC4.5/12) four times (averaged over multiple points). Simultaneously, samples were taken to measure the silicon content in molten iron using a spectrum analyzer (model: Thermo Scientific ARL4460). These two parameters were used as the model's output. The schematic diagram of the industrial trials is shown in Figure 1.

3. Data processing
3.1. Correlation analysis of influencing factors

Since there are numerous parameters affecting blast furnace production, the input parameters will directly impact the prediction accuracy for molten iron temperature and silicon content. To identify the
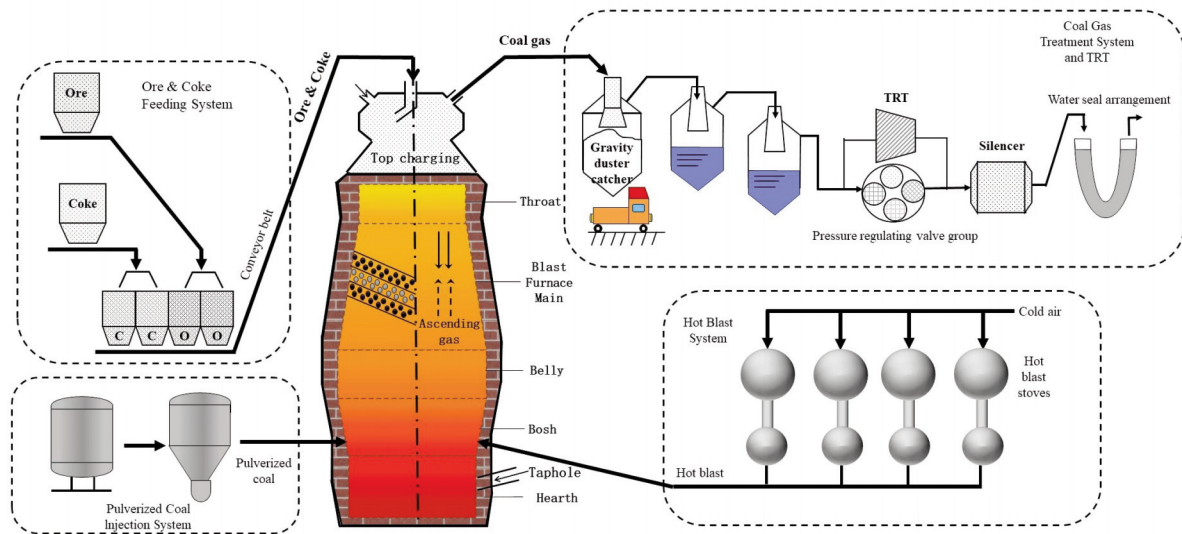
Figure 1. Schematic diagram of industrial trials

input variables for the model, 2000 sets of collected production data were utilized. Correlation analysis of the influencing factors was conducted using SPSS, and the results are presented in Table I. The correlation coefficient measures the strength of the relationship between two variables. A value of 1 indicates a perfect positive correlation, -1 indicates a perfect negative correlation, and 0 indicates no correlation. The closer the coefficient is to 0, the weaker the correlation. Therefore, parameters with low correlation were excluded from the analysis. The data comparison leads to an ordering of the correlations regarding the temperature of molten iron as follows: Hot-air blast temperature, Blast furnace bosh gas volume, Hot blast air pressure, Oxygen enrichment rate, Coal ratio, Coke load, Coke ratio, Comprehensive smelting intensity, Blast furnace air volume, Blast furnace top pressure, Comprehensive load, Coke smelting intensity, Comprehensive coke ratio, Air permeability index, Wind speed, Slag-iron ratio; Provides a basis for studying the factors affecting iron temperature. The correlation regarding iron silicon content is ranked as follows: Hot blast air pressure, Coke load, Hot-air blast temperature, Oxygen enrichment rate, Coal ratio, Blast furnace bosh gas volume, Comprehensive smelting intensity,

Table 1. Table of correlation coefficients between influencing factors

| Variable	Variable name	Molten iron temperature correlation coefficient	Molten iron silicon content correlation coefficient
X_1	Oxygen enrichment rate (%)	0.586	0.596
X_2	Comprehensive coke ratio	0.294	0.221
X_3	Wind speed (m·s^{-1})	-0.239	-0.448
X_4	Blast furnace bosh gas volume (m^3)	-0.614	-0.56
X_5	Coal ratio (kg·t^{-1})	0.519	0.503
X_6	Hot-air blast temperature (°C)	0.616	-0.637
X_7	Slag-iron ratio (kg·t^{-1})	-0.15	-0.124
X_8	Air permeability index	-0.261	-0.409
X_9	Blast furnace top pressure (MPa)	-0.358	-0.322
X_{10}	Blast furnace air volume (m^3·min^{-1})	-0.427	-0.471
X_{11}	Coke ratio (kg·t^{-1})	0.508	0.403
X_{12}	Hot blast air pressure (MPa)	-0.606	0.665
X_{13}	Comprehensive load	0.346	0.139
X_{14}	Coke load	-0.513	-0.647
X_{15}	Coke smelting intensity	0.302	0.375
X_{16}	Comprehensive smelting intensity	-0.484	-0.477
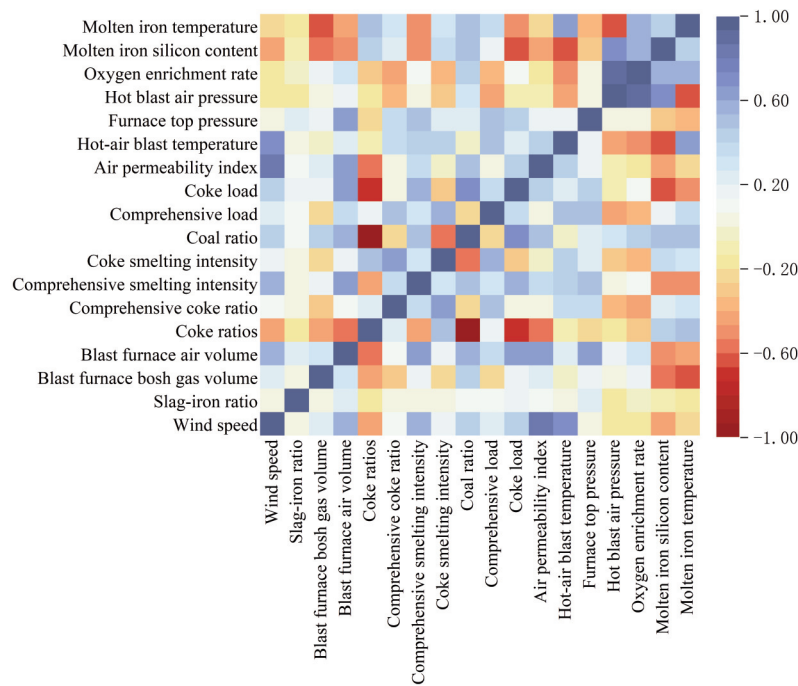
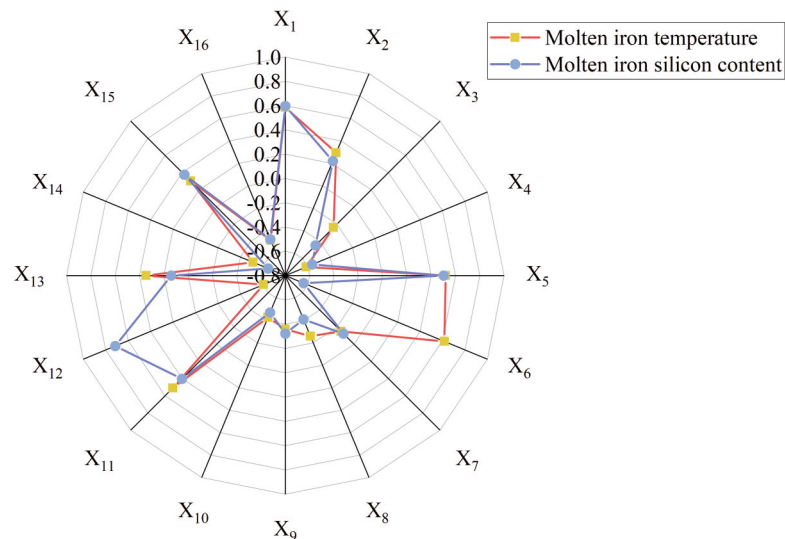**Figure 2.** *The correlation coefficient between the features*

Figure 3. *Radar chart for correlation analysis*

Blast furnace air volume, Wind speed, Air permeability index, Coke ratio, Coke smelting intensity, Blast furnace top pressure, Comprehensive coke ratio, Comprehensive load, Slag-iron ratio. Provides a basis for the study of the factors affecting the silicon content of molten iron. The correlation heat map between the factors is shown in Figure 2. The scale on the right side of the heat map indicates the color shades corresponding to different correlation coefficients. When the correlation between multiple

attributes is very high (correlation coefficient > 0.7), known as multicollinearity, it tends to result in unstable predictions. Variables with high correlation coefficients with multiple parameters are excluded, as correlation exists between most parameters. The correlation coefficients between the 16 influencing factors and molten iron temperature and silicon content are shown in Figure 3. In the Figure, closer proximity to the outer circle indicates a stronger positive correlation, while closer proximity to the

inner circle indicates a stronger negative correlation. The axes in the radial direction correspond to specific variables as shown in Table 1.

3.2. Data normalization

Due to the wide range of factors influencing blast furnace molten iron quality characteristics, the numerical variances are excessive. To increase the accuracy of the blast furnace molten iron quality parameter prediction model, facilitate rapid convergence, and enhance the model's generalization capacity, the input and output data are normalized using the following equations:

Step 1: Calculation of quartiles: Sort the dataset $X=\{x_1, x_2, \ldots, x_n\}$ to obtain x_{sort}, whereand satisfies $X_{sort}=\{x_{(1)}, x_{(2)}, \ldots, x_{(n)}\}$

The quantile q_i of each data point x_i can be calculated from its sort position r_i:

$$q_i = \frac{r_i}{n+1} \tag{1}$$

where r_i, is the position index of data point x_i after sorting and n is the total number of data points.

Step 2: Map the computed quantile q_i to the target distribution [0,1].

$$x_i' = q_i \tag{2}$$

4. Establishment of predictive model
4.1. Establishment of LAOA model

The AOA has the advantages of fast convergence speed and strong global search ability, but it has poor exploratory ability and tends to converge to non-optimal solutions prematurely. To solve this problem, the research group introduces random perturbation to the optimal position in AOA using Lévy flight, expanding the search range and accelerating convergence speed. The steps are as follows:

Step 1: With the introduction of the Lévy flight perturbation, the new optimal position is calculated as follows:

$$X^*(t) = X(t) + a*\text{Lévy}(\lambda) \tag{3}$$

where:

$X^*(t)$: Optimal individual generated by previous t iterations;

X(t): Current position vector;

a: Random number of optimal individual locations.

$$\text{Lévy}(\lambda): |\lambda|^{-1-\delta}, 0 < \delta < 2 \tag{4}$$

where:

λ: Random Lévy step.

Since the Lévy flight is complex, it is simulated using the Mantegna algorithm, which is mathematically formulated as follows:

$$\lambda = \frac{\mu}{|\kappa|^{\frac{1}{\delta}}} \tag{5}$$

where:

μ: $N(0, \sigma_\mu^2)$ and κ:N(0,1) obey uniform distribution.

$$\sigma_\mu = \frac{\Gamma(1+\beta)\sin\left(\frac{\pi\beta}{2}\right)}{\Gamma\left(\frac{1+\beta}{2}\right)\beta 2^{\left(\frac{\beta-1}{2}\right)}} \tag{6}$$

To reduce the calculation amount, β =1.5 is taken in the calculation process, then σ_μ= 0.6966.

Step 2: After defining the optimal search agent, other search agents will try to update the location to the best search agent, which is represented by the mathematical model:

$$MOA(C_{Iter}) = Min + C_{Iter} \times \left(\frac{Max - Min}{M_{Iter}}\right) \tag{7}$$

$$x_{i,j}(C_{Iter}+1) = \begin{cases} best(x_j) \div (MOP + \in) \times ((UB_J - LB_J) \times \mu + LB_J), r2 < 0.5 \\ best(x_J) \times MOP \times (UB_J - LB_J) \times \mu + LB_J, otherwise \end{cases} \tag{8}$$

where:

$MOA(C_{Iter})$: Value of the function at the t-th iteration. Function is a coefficient calculated by Eq. (6) used in the following search phases;

C_{Iter}: Current iteration, which is between 1 and the maximum number of iterations;

Min, Max: Minimum and maximum values of the acceleration function, respectively;

$x_i(C_{Iter}+1)$: The i-th solution in the next iteration;

$x_{i,j}(C_{Iter}+1)$: The j-th position of the i-th solution in the current iteration;

$best(x_j)$: The j-th position in the best solution obtained so far;

$\in$ is a small integer;

UB_J, LB_J : Upper and lower bound values for the j-th position, respectively.

$$MOP(C_{Iter}) = 1 - \frac{C\_Iter^{1/\alpha}}{M_{Iter}^{1/\alpha}} \tag{9}$$

where:

MOP(C_{Iter}): Value of the coefficient MOP at the current number of iterations;

α: A sensitive parameter reflecting the accuracy of mining for the number of iterations and is fixed to 5.

In the AOA, the exploration phase is limited by the boundaries of the design variables, which may lead to problems of poor exploration capability and premature convergence to non-optimal solutions. The use of Lévy to improve the AOA can be a good way to avoid this kind of problem, expand the exploration capability, and make the parameter converge to the optimal solution. The coefficients μ can be calculated by the following equation:

$$\mu = 2aL\acute{e}vy\lambda\text{-ae} \tag{10}$$

Step 3: In the exploitation phase, the operator can easily enhance the search process in the promising regions of the search space detected in the exploration phase, and the mathematical model of its position update can be expressed as follows:

$$x_{i,j}\left(C_{Iter}+1\right) =$$
$$\begin{cases} best\left(x_j\right) - MOP \times \left(\left(UB_J - LB_J\right) \times \mu + LB_J\right), r3 < 0.5 \\ best\left(x_j\right) + MOP \times \left(UB_J - LB_J\right) \times \mu + LB_J\right), otherwise \end{cases} \tag{11}$$

where:

r3: A uniformly distributed pseudo-random number with values ranging from 0 to 1.

4.2. Establishment of TSVR model

TSVR obtains the objective function by solving two quadratic programming problems to obtain two regression functions. Assuming that the training sample is an n-dimensional vector, it can be denoted as (x_1, y_1), ..., (x_p, y_p), the number of training samples is p. Let the input training samples A=$[x_1, ..., x_p]^T \in R^{p*n}$, the output training sample Y=$[y_1, ..., y_p]^T \in R^{p*n}$, a unit vector of appropriate dimension e=$[1, ...,1]^T$ [17] and introduce the kernel function as well as the regression function with the expression:

$$K\left(x^T, A^T\right) = \exp\left(-\frac{\left\|x^T - x_i^T\right\|^2}{2\sigma^2}\right), \sigma \rangle 0 \tag{12}$$

$$H = \left[K\left(A, A^T\right), e\right] \tag{13}$$

$$f_{w1}(x) = K\left(x^T, A^T\right)\omega_1 + b_1 \tag{14}$$

$$f_{w2}(x) = K\left(x^T, A^T\right)\omega_2 + b_2 \tag{15}$$

where:

σ: Width of the Gaussian kernel function;

ω_1, ω_2: Weight vectors;

b_1, b_2: Bias terms.

By introducing the Lagrange multiplier α, the β, combined with the KKT condition, the dyadic problem of the objective function can be obtained and solved to obtain the optimization problem of Eqs. (13) and (14).

$$\max(\frac{1}{2}\alpha^T H\left(H^T H\right)^{-1} H^T \alpha + f^T H\left(H^T H\right)^{-1} H^T \alpha - f^T \alpha) \tag{16}$$

$$f = Y - e\varepsilon_1, 0 \leq \alpha \leq C_1 e \tag{17}$$

$$\max(\frac{1}{2}\beta^T H\left(H^T H\right)^{-1} H^T \beta + h^T H\left(H^T H\right)^{-1} H^T \beta - h^T \beta) \tag{18}$$

$$h = Y - e\varepsilon_2, 0 \leq \beta \leq C_2 e \tag{19}$$

where:

$C_1, C_2, \varepsilon_1, \varepsilon_2$, f, h: Adjustment parameter;

α: A vector of Lagrange multipliers;

β: Lagrange multiplier vector.

Using the optimal solution obtained from the above equation, the first term in the objective function of the optimization problem is the sum of the squares of the distances from the training sample points to the function where the upper and lower bounds are located, so the optimal solution can be obtained by minimizing the first term such that the function $f_{w1}(x)$ or $f_{w2}(x)$ can be adapted to ε_1 or ε_2 where the training samples have to be larger than the function $f_{w1}(x)$ with a distance at least greater than ε_1, and the objective function $f_{w2}(x)$ has a distance at least less than ε_2, when there is a distance greater than ε_1 or ε_2 of error samples exists, they are penalized by the slack variables, and the weight vector and bias vector can be obtained as:

$$\left[\omega_1, b_1\right]^T = \left(H^T H + \gamma I\right)^{-1} H^T \left(f - \alpha\right) \tag{20}$$

$$\left[\omega_2, b_2\right]^T = \left(H^T H + \gamma I\right)^{-1} H^T \left(h + \beta\right) \tag{21}$$

where:

γ: Normal number;

I: A unit matrix of appropriate dimensions.

Then the values of the weight vector and bias are brought into the regression function $f_1(x)$ and $f_2(x)$ in which, using these two objective regression prediction functions, the prediction model can be determined according to the principle of the TSVR, which ultimately results in the objective function of the model:

$$f_w(x) = K\left(x^{\mathrm{T}}, A^{\mathrm{T}}\right)\frac{(\omega_1 + \omega_2)}{2} + \frac{(b_1 + b_2)}{2} \qquad (22)$$

4.3. Establishment of LAOA-TSVR model

2000 sets of data are randomly picked from the trials database, 1500 for training and 500 for testing. The LAOA-TSVR is used to establish the prediction models of iron temperature and molten iron silicon content, respectively, and its detailed optimization process is shown in Figure 4 with the settings lambda: 1.5, search solutions: 10, max iterations: 1000.

To produce the best prediction results, the LAOA is utilized to improve the kernel function, tuning parameters, and penalty factors of the TSVR model, resulting in the LAOA-TSVR model. The process of the LAOA-TSVR is illustrated in Figure. 4 with the following steps:

4.4. Modeling based on blast furnace molten iron temperature prediction

Figures 5(a) and 5(b) illustrate the prediction results of the blast furnace molten iron temperature prediction model for the training and test datasets. These figures compare the predicted and actual iron temperatures for 1500 training samples and 500 test samples, respectively. As shown in the plots, the predicted values align closely with the actual values, exhibiting minimal differences. This demonstrates that the model achieves satisfactory prediction performance.

4.5. Modeling based on blast furnace molten iron t silicon content

To evaluate the predictive performance of the model, the developed blast furnace iron-silicon content prediction model was evaluated using both the training and test datasets. Figures 6(a) and 6(b) display the prediction results for the training and test datasets of the blast furnace iron-silicon content prediction model, respectively. The simulation results indicate that the predicted values closely follow the trend of the actual values, with minimal differences. This demonstrates that the developed model achieves satisfactory predictive performance.
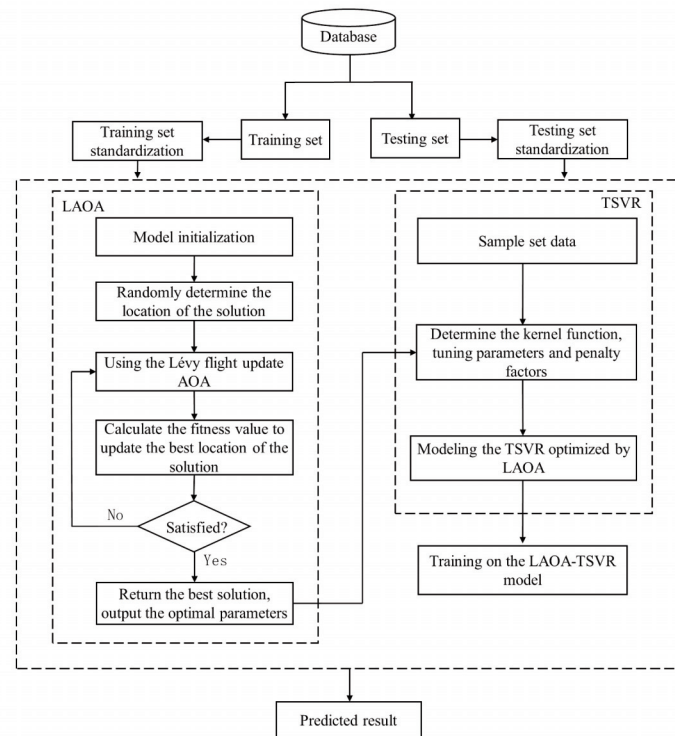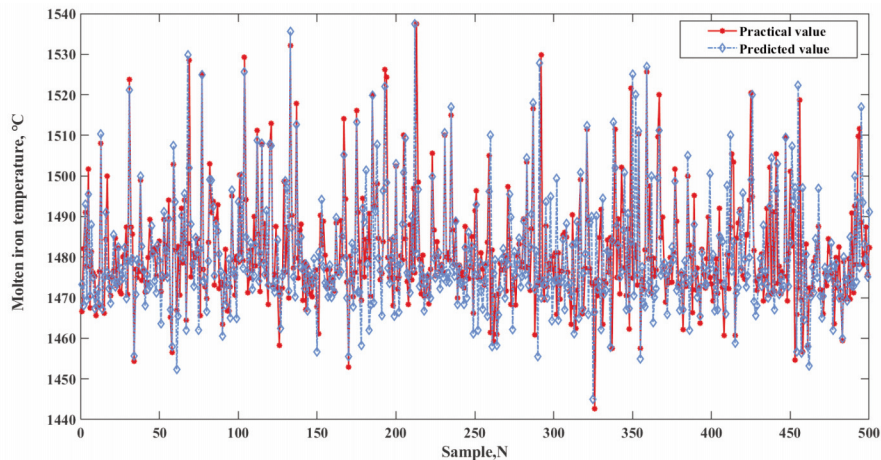

Figure 4. *Flow chart of the LAOA-TSVR model*

Table 2. *Algorithm steps*

Steps	Element
Step 1	The database is utilized to obtain the training set and test set samples and the data is preprocessed
Step 2	The model is initialized to randomly determine the location of a solution
Step 3	Using the Lévy flight update arithmetic optimization algorithm, calculate the fitness value to update the best solution and obtain the optimal solution vector
Step 4	Calculate whether the end condition is met to reach the maximum number of itera-tions 1000 times, if so, output the best parameters. Otherwise, continue to iterate and update according to the arithmetic optimization algorithm until the end condition is met
Step 5	Substitute the optimal vectors into the weight vectors and deviation vectors to obtain the kernel function, tuning parameters and penalty factors
Step 6	The LAOA-TSVR prediction model is built
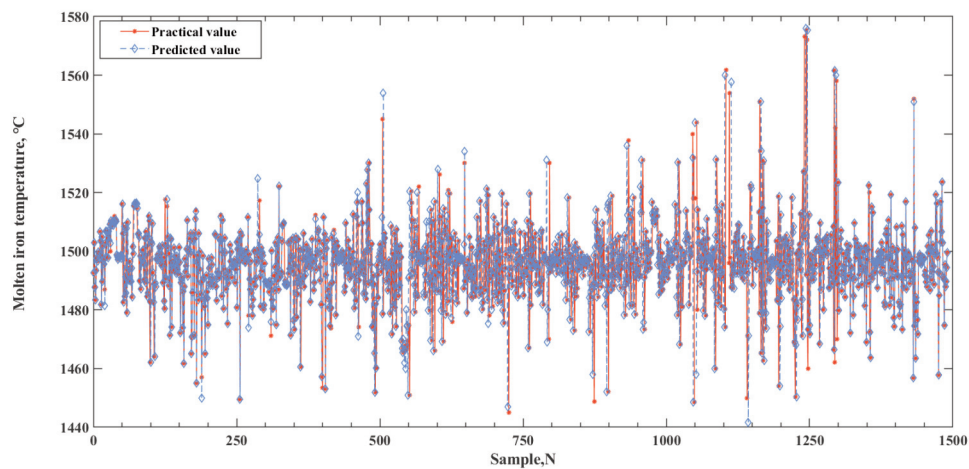
Figure 5a. *Comparison of training set and actual values of iron temperature*

Figure 5b. *Comparison of the test set and actual values of iron temperature*

5. Comparison of models and analysis of results
5.1. Comparison of model prediction effects

To verify the effect of the LAOA-TSVR model. It is compared with three algorithms models: BP (learning rate: 0.05, max training iterations: 1000, required accuracy: 1e-5, min error: 0.005), SVR (kernel='rbf',degree=3, gamma='auto_deprecated', coef0=0.0, tol=0.001, C=1.0, epsilon=0.1,
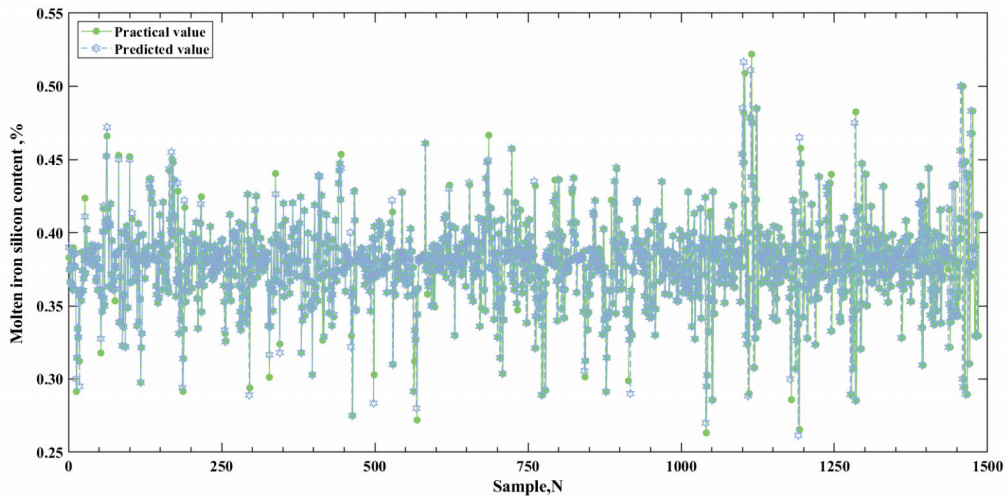
Figure 6a. *Comparison of the training set and actual values of molten iron silicon content*
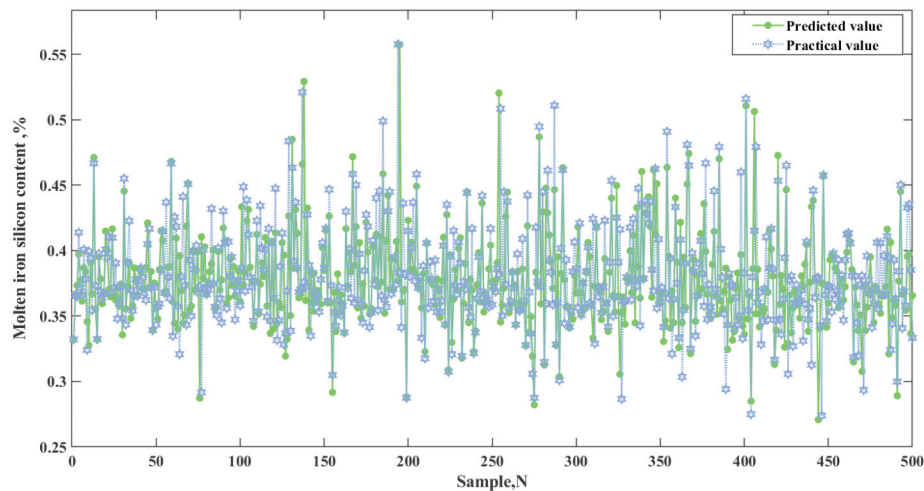

Figure 6b. *Comparison of the test set and actual values of molten iron silicon content*

shrinking=True, probability=False, cache_size=200, verbose=False, max_iter=-1, class_weight=None, decision_ function_ shape='ovr', random_state=None) and TSVR(Epsilon1=0.1, Epsilon2=0.1, C1=1, C2=1, kernel_type=0, kernel_param=1, regulz1=0.0001, regulz2=0.0001,estimator_type="regressor"). The error distributions of the predicted and actual values of the four models were determined as shown in Figure 7 and Figure 8.

5.2. Comparative analysis of models

To correctly assess the predicting performance of the LAOA-TSVR model, the research group employed SSR/SST and SSE/SST to calculate the model's fitting result. The closer the SSR / SST value is to 1, the closer the model prediction value is to the real value's amount of fluctuation; and the lower the

SSE /SST value, the better the model prediction value matches the genuine value. Then in order to verify the prediction effect of the constructed model more comprehensively, the LAOA-TSVR model was compared with the three models of BP, SVR and TSVR. MAE and RMSE were used as error indicators to analyze the accuracy of the model, and the results of the comparison of the prediction performance of iron temperature and iron silica content are shown in Table 3.

$$SSE / SST = \sum_{i=1}^{m} \frac{(y_i - \check{y}_i)^2}{\sum_{i=1}^{m}(y_i - \overline{y_i})^2} \tag{23}$$

$$SSE / SST = \sum_{i=1}^{m} \frac{(\check{y}_i - \overline{y_i})^2}{\sum_{i=1}^{m}(y_i - \overline{y_i})^2} \tag{24}$$
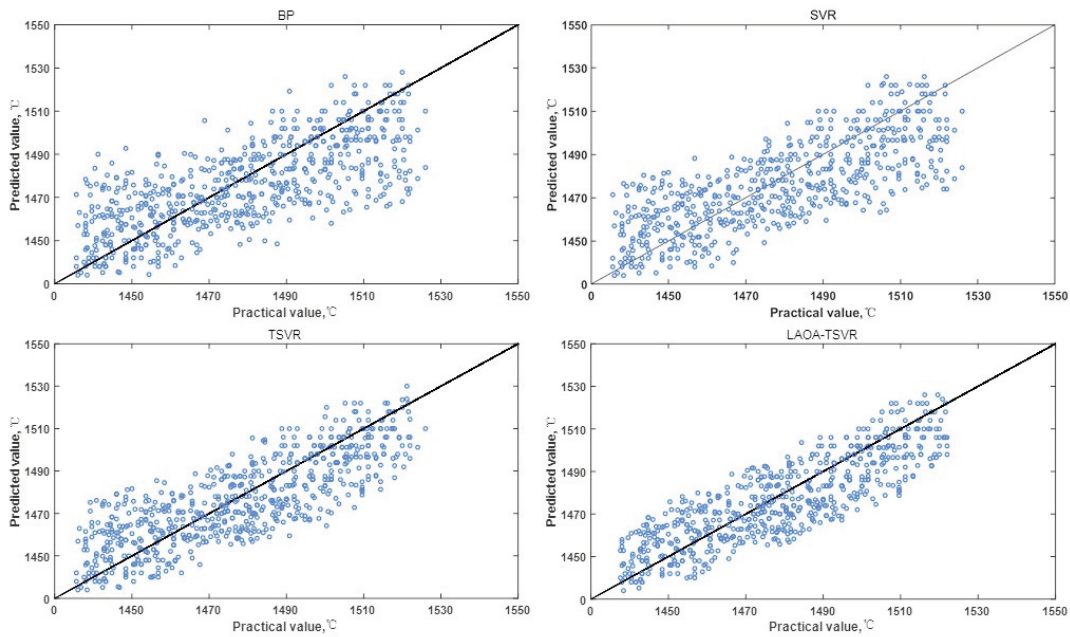
Figure 7. *Comparison of error between predicted and actual values of molten iron temperature for different models*
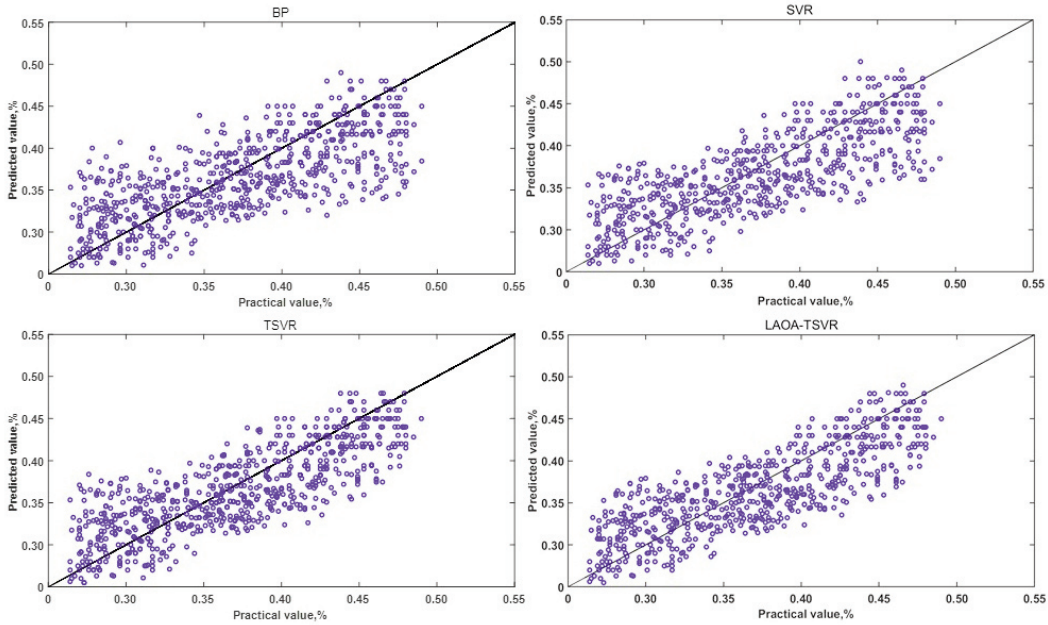

Figure 8. *Comparison of errors between predicted and actual values of molten iron silicon content for different models*

$$\text{MAE} = \frac{1}{m} \sum_{i=1}^{m} \left| \check{y}_i - y_i \right| \qquad (25)$$

$$RMSE = \sqrt{\frac{1}{m} \sum_{i=1}^{m} (y_i - \check{y}_i)^2} \qquad (26)$$

where:
m: Number of samples;

y_i: Actual value of the test sample;
$\overline{y}_i$: Mean value of the test sample;
$\check{y}_i$: Predicted value of the mode.

Table 3 demonstrates that the SSR/SST values of the four methods (BP, SVR, TSVR, and LAOA-TSVR) increase in turn while the SSE/SST values decrease. The LAOA-TSVR model has the greatest fitting degree and prediction precision.

To determine the extent to which the model met

Table 3. Evaluation indicators for the model

Model	Index	BP	SVR	TSVR	LAOA-TSVR
Prediction model of molten iron temperature	SSR/SST	0.62	0.67	0.78	0.91
	SSE/SST	0.74	0.65	0.57	0.3
	RMSE	12.55	11.45	10.38	8.94
	MAE	13.86	10.66	9.83	6.05
Prediction model of molten iron silicon content	SSR/SST	0.61	0.67	0.75	0.9
	SSE/SST	0.76	0.67	0.59	0.31
	RMSE	0.03	0.03	0.02	0.01
	MAE	0.03	0.02	0.01	0.01

the aim, the task force utilized HR performance metrics to calculate the prediction accuracy of the models, as illustrated in Figure 9 and Figure 10.

$$P_S * (100\% - k) < P_y < P_S * (100\% + k) \quad (27)$$

where:

P_S: Actual blast furnace iron temperature and molten iron silicon content;

P_y: Predicted blast furnace molten iron temperature and molten iron silicon content;

K: Accuracy rate of 5%, 0.5%.

$$HR = \frac{\left(\left| y_i - \frac{\wedge}{y_i} \right| \le n_e \right)}{n} *100\% \quad (28)$$

Figure 9 and Figure 10 show that the model for predicting blast furnace molten iron temperature within a ±5% error range has the following ratio from high to ground: LAOA-TSVR, TSVR, SVR, BP, and the prediction rate for the molten iron silicon content within the errors range ± 0.5% from high-to-ground, the following: LAOA-TSVR, TSVR, SVR, BP. This means that the model has a greater predictive effect than other models under the same conditions.
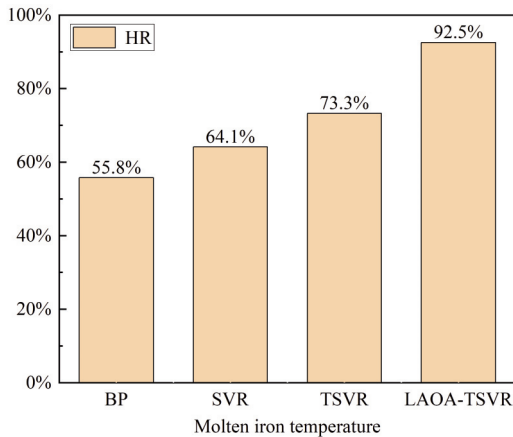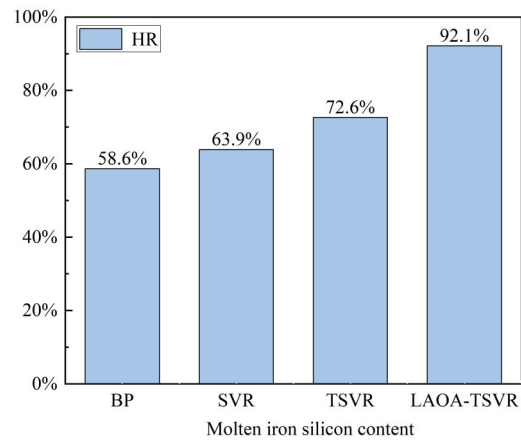

Figure 10. Hit rate of molten iron silicon content prediction model using four algorithms

6. Application and Validation

To verify the practical application effect of the established LAOA-TSVR prediction model, the model was applied to the actual production process of blast furnace in an iron mill for a total of 200 furnaces, and the results are shown in Figure 11 and Figure 12. According to the final hit rate, we know that the hit rate of blast furnace molten iron temperature and
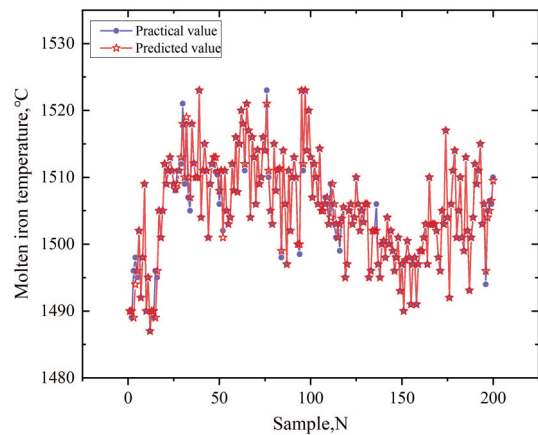

Figure 9. Hit rate of molten iron temperature prediction model using four algorithms

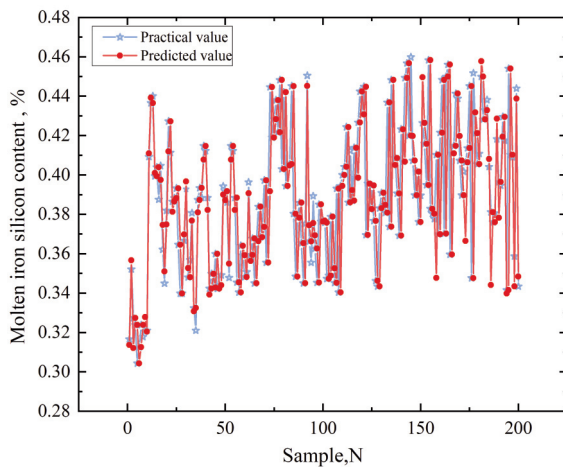*Figure 11. Practical application effect of molten iron temperature prediction model*

Figure 12. Practical application effect of molten iron silicon content prediction model

molten iron silicon content within the error range of ±5% and ±0.5% are 92.12% and 92.53%, respectively, and the corresponding double hit rate is 85.32%. The results can well meet the actual production needs of an iron mill and can provide guidance for actual production.

7. Conclusion

Based on the working conditions of actual blast furnace production, a model for predicting the temperature of silicon content of the molten iron of blast furnace based on LAOA-TSVR was established, and the conclusions are as follows:

(1) The proposed LAOA-TSVR model addresses the problems of low accuracy and many local optimal solutions in predicting the temperature and silicon content of the molten iron of blast furnace in traditional research, and at the same time improves the prediction accuracy, generalization ability and working speed of the model.

(2) The LAOA-TSVR model was applied to the actual production of 200 furnaces. The results show that the hit rates for the temperature of molten iron in the blast furnace and the silicon content of the molten iron are within ±5% and ±0.5% at 92.12% and 92.53%, respectively. The corresponding double hit rate (both parameters are met at the same time) is 85.32%.

(3) The comparison of the prediction effects of the three typical models shows that the LAOA-TSVR model has the highest evaluation index. This indicates that the LAOA-TSVR model has the best prediction performance and can provide practical production guidance for a blast furnace.

Author's contributions

Conceptualization, C.S. and P.T.; methodology, C.S. and P.T.; software, P.T.; validation, L.Z.; formal analysis, Y.W.; investigation, P.T.; resources, C.S.; data curation, S.L.; writing—original draft preparation, P.T.; writing—review and editing, C.S. and P.T.; visualization, Y.W.; supervision, C.S. and L.Z.; project administration, C.S.; funding acquisition, C.S. All authors have read and agreed to the published version of the manuscript.

Data Availability Statement

The raw/processed data required to reproduce these findings can-not be shared at this time as the data also forms part of an ongoing study.

Conflict of Interest

The authors declare no conflict of interest.

References

[1] S. Gupta, D. French, R. Sakurovs, M. Grigore, H. Sun, T. Cham, T. Hilding, M. Hallin, B. Lindblom, V. Sahajwalla, Minerals and iron-making reactions in blast furnaces, Progress in Energy and Combustion Science, 34 (2) (2008) 97. https://doi.org/10.1016/j.pecs.2007.04.001.

[2] X. Liu, L. Chen, H. Feng, X. Qin, F. Sun, Constructal design of a blast furnace iron-making process based on multi-objective optimization, Energy, 109 (2016) 137-151. https://doi.org/10.1016/j.energy.2016.04.101

[3] G. Deodatis, M. Shinozuka, Auto-regressive model for nonstationary stochastic processes, Journal of Engineering Mechanics, 114 (11) (1988) 01. https://doi.org/10.1061/(ASCE)0733-9399(1988)114:11(1995)

[4] R. Ostermark, H. Saxen, VARMAX-modelling of blast furnace process variables, European Journal of Operational Research, 90 (1) (1996) 85-101. https://doi.org/10.1016/0377-2217(94)00304-1

[5] J. Chen, A predictive system for blast furnaces by integrating a neural network with qualitative analysis, Engineering Applications of Artificial Intelligence, 14

(1) (2001) 77-85.
https://doi.org/10.1016/S0952-1976(00)00062-2

[6] W. Chen, B. Wang, H. Han, Prediction and control for silicon content in pig iron of blast furnace by integrating artificial neural network with genetic algorithm, Ironmaking & Steelmaking, 37 (6) (2010) 458-463. https://doi.org/10.1179/174328109X445769

[7] S. Barik, R. Bhandari, M.K. Mondal, Optimization of wire arc additive manufacturing process parameters for low-carbon steel and properties prediction by support vector regression model, Steel Research International, 95 (1) (2024). https://doi.org/10.1002/srin.202300369

[8] S.M. Acosta, A.L. Amoroso, Â.M.O. Sant'Anna, O.C. Junior, Predictive modeling in a steelmaking process using optimized relevance vector regression and support vector regression, Annals of Operations Research, 316 (2022) 905–926. https://doi.org/10.1007/s10479-021-04053-9

[9] C. Giannetti, E. Borghini, A. Carr, J. Raleigh, B. Rackham, Deep learning for robust forecasting of hot metal silicon content in a blast furnace, The International Journal of Advanced Manufacturing Technology, 131 (9-10) (2024) 4403-4423. https://doi.org/10.1007/s00170-024-13214-6

[10] C. Shi, B. Wang, J. Chen, R. Zhong, S. Guo, P. Sun, Bending force of hot rolled strip based on improved whale optimization algorithm and twinning support vector machine, Metals, 12 (10) (2022) 1589. https://doi.org/10.3390/met12101589

[11] C. Shi, S. Guo, J. Chen, R. Zhong, B. Wang, P. Sun, Z. Ma, Breakout prediction based on twin support vector machine of improved whale optimization algorithm. ISIJ International, 63 (5) (2023) 880-888. https://doi.org/10.2355/isijinternational.ISIJINT-2022-372

[12] C. Shi, S. Guo, B. Wang, X. Yin, P. Sun, Y. Wang, L. Zhang, R. Chen, Z. Ma, The forcast of slag addition during the ladle furnace (LF) refining process based on LWOA-TSVR, Metalurgija, 62 (2) (2023) 197-200.

[13] L. Abualigah, A. Diabat, S. Mirjalili, A. Mohamed, A. Gandomi, The arithmetic optimization algorithm, Computer Methods in Applied Mechanics and Engineering, 376 (2021) 113609. https://doi.org/10.1016/j.cma.2020.113609

[14] J. Li, Q. An, H. Lei, Q. Deng, G.Wang, Survey of Lévy flight-based metaheuristics for optimization, Mathematics, 10 (15) (2022) 2785. https://doi.org/10.3390/math10152785

[15] H. Haklı, H. Uğuz, A novel particle swarm optimization algorithm with Levy flight, Applied Soft Computing, 23 (2014) 333-345. https://doi.org/10.1016/j.asoc.2014.06.034

[16] J. Xue, B. Shen, A novel swarm intelligence optimization approach: sparrow search algorithm, Systems Science & Control Engineering, 8 (1) (2020) 22–34. https://doi.org/10.1080/21642583.2019.1708830

[17] X. Peng, TSVR: An efficient twin support vector machine for regression, Neural Networks, 23 (3) (2010) 365-372. https://doi.org/10.1016/j.neunet.2009.07.002

MODEL PREDIKCIJE TEMPERATURE RASTOPLJENOG ŽELEZA U VISOKOJ PEĆI I SADRŽAJA SILICIJUMA U RASTOPLJENOM ŽELEZU ZASNOVAN NA UNAPREĐENOM ALGORITMU ARITMETIČKE OPTIMIZACIJE ZA TSVR MAŠINU

C.-Y. Shi [a],* P.-L. Tao [a], S.-D. Li [b], Y.-K. Wang [a], L. Zhang [a]

[a] Fakultet elektrotehnike i inženjeringa automatizacije, Ljaoning institut nauke i tehnologije, Bensi, Kina
[b] Odeljenje za specijalni čelik, Benxi Steel Plate Co., Bensi, Kina

Apstrakt

Temperatura i sadržaj silicijuma u rastopljenom železu iz visoke peći direktno su povezani s njegovim kvalitetom. Stoga je kreiranje efikasnog modela za predikciju ovih parametara od ključnog značaja. Kako bi se odgovorilo na ove izazove, razvijen je model sa unapređenim algoritmom aritmetičke optimizacije za TSVR mašinu (LAOA-TSVR) za predikciju temperature i sadržaja silicijuma u rastopljenom železu iz visoke peći. Prvo, korišćenjem SPSS-a sprovedena je analiza korelacije radi identifikacije glavnih faktora uticaja. Zatim je model upoređen sa tri uobičajena modela za predikciju radi verifikacije performansi: neuronskom mrežom sa povratnim širenjem (BP), regresijom sa mašinom podrške (SVR) i TSVR mašinom. Preliminarni rezultati pokazuju da je tačnost predikcije modela LAOA-TSVR značajno veća u poređenju sa drugim modelima. Na kraju, model je primenjen u stvarnom proizvodnom procesu u železari na uzorku od 200 visokopećnih procesa. Rezultati pokazuju da su stepeni uspešnosti za temperaturu rastopljenog železa i sadržaj silicijuma unutar greške od ±5% i ±0,5% na nivou od 92,12% i 92,53%, respektivno, dok je dvostruki stepen uspešnosti 85,32%. Model efikasno ispunjava proizvodne zahteve železare i pruža dragocene informacije za proizvodni proces visoke peći.

Ključne reči: Temperatura rastopljenog železa u visokoj peći; Sadržaj silicijuma u rastopljenom železu; Kvalitet rastopljenog železa; Algoritam aritmetičke optimizacije; TSVR mašina